Analytical and Bioanalytical Chemistry
https://doi.org/10.1007/s00216-019-01743-z

RESEARCH PAPER

Monocrotophos detection with a bienzyme biosensor based on ionic-liquid-modified carbon nanotubes

Bin Zou[1] · Yanhong Chu[1] · Jiaojiao Xia[1]

Received: 1 December 2018 / Revised: 1 February 2019 / Accepted: 28 February 2019

Abstract

Acetylcholinesterase (AChE) biosensor technology is widely applied in the detection of organophosphate pesticides in agricultural production via the inhibition of AChE activity by organophosphates. However, the AChE electrode has some drawbacks, such as low stability and high overpotential. Combining the advantages of multiwalled carbon nanotubes (MWCNTs) and ionic liquids, we constructed a novel bienzyme electrode [Cl/iron porphyrin (FePP)-modified MWCNTs/AChE/glassy carbon electrode], which included AChE and mimetic oxidase FePP. In this electrode, FePP is covalently bound to the AChE carrier via ionic liquid for increased electrode sensitivity and stability. Under optimal conditions, this novel biosensor has a monocrotophos detection limit of 3.2×10^{-11} mol/L and good recovery of 89–104%. After 5 weeks of storage at 4 °C, the oxidation current was 97.8% of its original value. The biosensor has high stability and sensitivity for monocrotophos detection and is a promising device for monitoring food safety.

Keywords Acetylcholinesterase · Mimetic oxidase · Modification · Ionic liquids · Monocrotophos

Introduction

Organophosphates are widely used in agricultural production because of high insecticidal activity. However, organophosphates can also bind to hydroxyl groups on serine, which is part of the active center of acetylcholinesterase (AChE). Because of this interaction, AChE loses the hydrolytic capacity of acetylcholine, resulting in activity disorder of the cholinergic receptor and even death [1]. To protect human health, it is thus of great importance to promote the detection of organophosphate residues in agricultural products. Traditional detection methods such as gas chromatography [2], liquid chromatography [3], and mass spectrometry [4] have been widely used in the detection of organophosphates, but these methods are not suitable for large-scale and fast detection because of common shortcomings such as huge equipment, long measurement time, and high cost [5].

Biosensor technology has gradually replaced traditional organophosphate detection methods because of simple and fast operation and high selectivity. Electrode-immobilized AChE catalyzes the hydrolysis of acetylthiocholine chloride (ATCl) to generate the electroactive product thiocholine [6]. The organophosphate content is determined by measuring the decrease in the activity of AChE on organophosphate treatment [7]. The residual organophosphate amount is obtained by monitoring the thiocholine oxidation. However, this oxidation requires a suitable electrode carrier surface and an oxidation catalyst [8].

Multiwalled carbon nanotubes (MWCNTs) have been widely used as a "wire" for the electron transfer in enzyme biosensors [9–11]. However, the original MWCNTs tend to aggregate. After chemical modification, the MWCNT surface provides a large number of functional groups such as $–NH_2$ and –COOH [12]. These functional groups not only improve the dispersion of MWCNTs but also accelerate the electron transfer between the redox-active compound and the electrode [13]. Yu et al. [14] found that MWCNT-NH_2–AChE has high affinity for ATCl with a low Michaelis constant (K_M) 6.7×10^{-5} mol/L and a low paraoxon detection limit of 8×10^{-10} mol/L.

Electronic supplementary material The online version of this article (https://doi.org/10.1007/s00216-019-01743-z) contains supplementary material, which is available to authorized users.

✉ Bin Zou
binzou2009@ujs.edu.cn

✉ Jiaojiao Xia
jiaojiaoxia@ujs.edu.cn

[1] Jiangsu University, No.301 Xuefu Road, Zhenjiang 212013, Jiangsu, China

Published online: 22 April 2019

In recent years, ionic-liquid-functionalized materials have been widely used in biochemistry, and reports indicate that ionic liquids are highly compatible with enzymes and substrates and greatly increase enzyme activity and stability. On the other hand, ionic liquids exhibit good electrical conductivity and improve the dispersion of MWCNTs [15].

Furthermore, a suitable oxidase catalyst is another key factor for thiocholine oxidation, as this could amplify the current signal. In the detection of organophosphates, the choline oxidation signal increases when Au or Pd nanoparticles [16] or horseradish peroxidase (HRP) [17] is added to the AChE electrode. However, HRP is expensive and has low stability. Iron porphyrin (FePP) is the active center of HRP. Biomimetic oxidase FePP has excellent oxidation properties that are similar to those of HRP, although FePP is stabler than HRP [18]. Ji et al. [19] found that metal porphyrins are efficient catalysts for the oxidation of benzyl alcohol, with both conversion and selectivity greater than 95%.

In this study, we present a biosensor for the detection of organophosphates that combines the previously mentioned advantages of MWCNTs and ionic liquids and also includes AChE and low-cost FePP. Firstly, MWCNTs were in situ functionalized with ionic liquid. Secondly, FePP was covalently bound to the ionic-liquid-functionalized MWCNTs. Finally, AChE was added to obtain the novel bienzyme electrode. The biosensor developed was expected to exhibit high stability and sensitivity for organophosphate detection.

Experimental

Materials

OH-MWCNTs (purity greater than 95%, length 0.5–2 μm) were purchased from Beijing DK Nano Technology Co., monocrotophos (99.4%) was purchased from Beijing Putian Tongchuang Biotechnology Co., and AChE (C3389, 500 U mg^{-1}) and ATCl were purchased from Sigma-Aldrich (USA). Acetone, potassium hexacyanoferrate(III), ferric chloride, chloroform, and *N*,*N*-dimethylformamide (DMF) were purchased from Sinopharm Chemical Reagent Co. Chloropropyltriethoxysilane and 5,10,15,20-tetra(4-pyridyl)porphyrin (referred to as "porphyrin") were purchased from Shanghai Aladdin Biochemical Technology Co. Double-distilled water was used for all experiments, and all other reagents were of analytical grade and used without further purification.

Preparation of ionic-liquid-modified MWCNTs and immobilized FePP

Firstly, 0.5 g OH-MWCNTs and 2.4 g chloropropyltriethoxysilane were added to a conical flask containing 100 mL chloroform. The resulting suspension was treated by ultrasound for 15 min and stirred for 7 days at room temperature [20]. Subsequently, the suspension was centrifuged to remove the supernatant, and the precipitate was dried to obtain Cl-MWCNT powder.

Secondly, anhydrous $FeCl_3$ and porphyrin (molar ratio 5:1) were added to a round-bottom flask containing 50 mL DMF, and the resulting mixture was refluxed at 160 °C for 12 h [21]. After cooling to room temperature, the reaction mixture was filtered and centrifuged. Unreacted iron ions were removed from the filtered solid by successive dispersion in absolute ethanol and water followed by centrifugation. After repeated centrifugation and washing, the resulting solid was dried to obtain FePP powder.

Finally, 0.8 g Cl-MWCNTs and 20 mg FePP were added to a round-bottom flask containing 25 mL DMF, and the resulting solution was refluxed at 160 °C for 24 h [22]. The resulting black mixture was centrifuged and treated with chloroform to obtain the target carrier Cl/FePP-MWCNTs.

Preparation of AChE biosensor

Electrodes were polished with alumina slurries (0.10 and 0.05 μm) and sonicated in distilled water for 15 min. Then 10 mg carrier was mixed with 1 mL phosphate-buffered saline (PBS; pH 7.0), and carrier dispersion was obtained after sonication for 15 min. Next, 5 mg AChE powder was dissolved in 60 mL tris(hydroxymethyl)aminomethane–HCl (pH 7.0) by sonication for 15 min. Firstly, 10 μL carrier dispersion was dropped onto the bare electrode surface and dried with an infrared lamp at about 30 °C for 20 min. Then 10 μL enzyme solution was dropped onto this electrode and dried with an infrared lamp for another 20 min to obtain the Cl/FePP-MWCNTs/AChE/glass carbon electrode (GCE) biosensor. This modified electrode was stored at 4 °C until further use. For comparison, we also prepared the following electrodes: OH-MWCNTs/AChE/GCE, Cl-MWCNTs/AChE/GCE, porphyrin/AChE/GCE, and FePP/AChE/GCE.

Electrochemical detection of monocrotophos

The electrochemical properties of the modified electrodes were determined by cyclic voltammetry (CV) and electrochemical impedance spectroscopy (EIS) in 5.0 mmol/L $[Fe(CN)_6]^{3-/4-}$ solution. Monocrotophos was detected with this biosensor by differential pulse voltammetry (DPV). For monocrotophos measurement, the prepared biosensor was immersed in monocrotophos standard solution of various concentrations for 10 min. Afterward, the electrode surface was carefully washed with PBS (pH 7.0). DPV curves of the biosensor were obtained in PBS (pH 7.0) containing ATCl at 1.0

mmol/L. The monocrotophos inhibition rate was calculated according to the following equation:

$$I(\%) = \frac{i_1 - i_2}{i_1} \times 100\%,$$

where I is the inhibition rate of the enzyme, i_1 is the peak current of the sensor before incubation with monocrotophos, and i_2 is the peak current of the sensor after incubation with monocrotophos [23].

Monocrotophos residue detection in real samples

Cabbage, lettuce, and leek were washed three times with distilled water and then chopped. Five grams of each sample was sprayed with a certain concentration of standard monocrotophos pesticide, and then 10 mL mixed solution (0.1 mol/L acetone solution and pH 7.0 PBS, 1:9, v/v) was added [24]. This mixture was sonicated for 15 min, and the resulting suspension was centrifuged at 5000 rpm for 10 min. The supernatant was measured directly without extraction, and the monocrotophos concentration in the sample was calculated from the calibration curve by the standard addition method.

Apparatus

Fourier transform infrared spectroscopy was performed with a Nicolet-460 instrument (Thermo Fisher, USA) by the standard KBr disk method. About 20 mg sample powder was mixed with KBr to make a tablet and was scanned in the wavelength range from 400 to 4000 cm^{-1} with a resolution of 0.4 cm^{-1}. Scanning electron microscopy was performed with JSM-7500F microscope from JEOL. A small sample was stuck on conductive adhesive and sprayed with gold. The sample was studied at 30 kV with a resolution of 1.4 nm. A specific surface area test (Brunauer–Emmett–Teller) was performed with a Micro TriStar II Plus 2.02 apparatus at -196 °C. About 100 mg powder was degassed at 100 °C for 6 h. X-ray diffraction was performed with a D8 diffractometer (Bruker, Germany) with a voltage of 40 kV and a current of 40 mA. The scanning speed was 10°/min, the test range was 5° to 90°, and the step was 0.02°. Elemental analysis was performed with a Flash 2000 instrument from Thermo Fisher. The sample was placed in a combustion reactor and was burned in a pure oxygen atmosphere. The sample was completely converted to gas and was detected with a chromatographic column and a thermal conductivity detector. Inductively coupled plasma atomic emission spectrometry was performed with an Agilent 720 System. One hundred milligrams of sample powder was weighed for dissolution in mixed acid and diluted before being tested. CV and DPV were performed with a chi660D electrochemical workstation (Shanghai Chenhua Co., China). All experiments were performed with a three-electrode system at room temperature (a GCE was the working electrode, a Ag/AgCl electrode was the reference electrode, and a platinum wire electrode was the counter electrode).

Results and discussion

Material characterization

The surface morphologies of different modified surfaces were observed by scanning electron microscopy. Figure 1a shows the surface morphology of OH-MWCNTs, revealing that randomly distributed MWCNTs formed a uniform porous network structure, and the MWCNTs were excellently dispersed. Figure 1b reveals that the average diameter of OH-MWCNTs was 35.6 nm. Figure 1c shows the surface morphology of Cl-MWCNTs, revealing that some of the carbon nanotubes formed aggregates, which may be due to electrostatic attraction between the nanotubes after chloropropyltriethoxysilane modification. Figure 1d shows the surface morphology of FePP-MWCNTs, revealing that most of the iron was successfully loaded onto MWCNTs to form a dense film, and also vaguely the boundary between reticular and membranous structures. On encapsulation of FePP, MWCNTs act as a "molecular conductor" by forming electron transfer channels that connect the active center of AChE and the surface of the GCE. Figures S1 and S2 depict Fourier transform infrared spectra and X-ray diffraction patterns of different materials, indicating that AChE and FePP were successfully immobilized on the MWCNTs.

Table S1 shows that MWCNTs have a large specific surface area, as calculated from the N_2 adsorption curves presented in Fig. S3, providing many active sites for the loading of FePP. The specific surface area, pore volume, and pore size of the FePP-MWCNTs were smaller than those of the OH-MWCNTs because of the introduction of FePP into the MWCNT channels. The specific surface area of the OH-MWCNTs was 1.6 times higher than that of the FePP-MWCNTs, indicating that the OH-MWCNTs have greater adsorption capacity and compatibility with FePP [25]. Table S2 shows the Si, Fe, and N mass percentages of the FePP-MWCNT samples resulting from elemental analysis. Chloropropyltriethoxysilane and FePP accounted for about 3.90 wt% (calculation based on the Si content) and 12.02 wt % (calculation based on the Fe content) of the total sample mass, respectively.

Electrochemical behavior of the Cl/FePP-MWCNTs/GCE

The electrochemical properties of electrodes modified with different materials were compared by CV. CV was

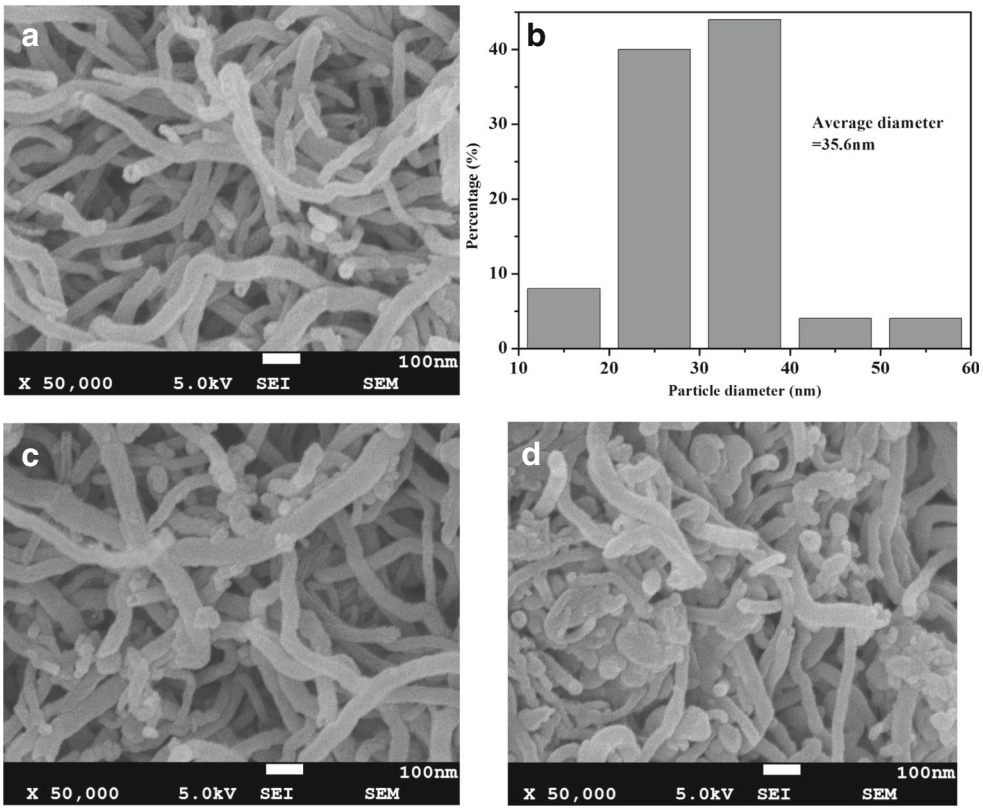

Fig. 1 Scanning electron microscopy images of **a** OH-modified multiwalled carbon nanotubes (MWCNTs), **c** Cl-modified MWCNTs, and **d** Cl/iron porphyrin modified MWCNT. **b** Average diameter of OH-modified MWCNTs,

sequentially performed on the OH-MWCNTs/GCE, Cl–MWCNTs/GCE, porphyrin/GCE, FePP/GCE, and Cl/FePP–MWCNTs/GCE in PBS (pH 7.0) containing $[Fe(CN)_6]^{3-/4-}$ at 5.0 mmol/L and KCl at 0.1 mol/L. Figure 2 shows that all

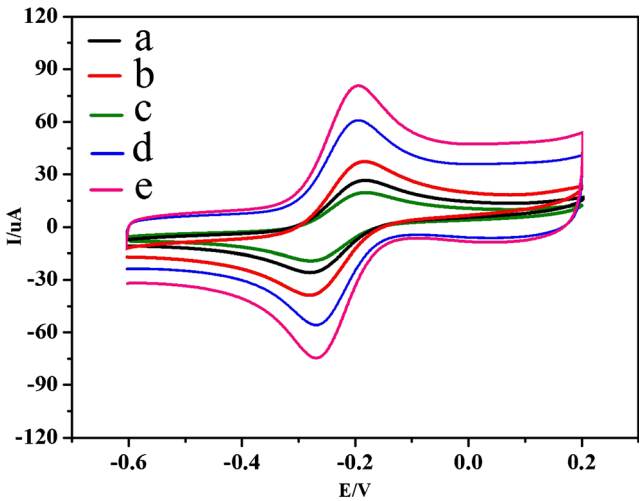

Fig. 2 Cyclic voltammograms of OH-modified multiwalled carbon nanotubes (MWCNTs)/glassy carbon electrode (GCE) (a), Cl-modified (MWCNTs)/GCE (b), porphyrin/GCE (c), iron porphyrin (FePP)/GCE (d), and Cl/FePP-modified MWCNTs/GCE (e) in 0.1 mol/L phosphate-buffered saline (pH 7.0) containing $[Fe(CN)_6]^{3-/4-}$ at 5.0 mmol/L KCl at and 0.1 mol/L

modified electrodes exhibited clear redox peaks in the range from –0.6 to 0.2 V. Compared with OH-MWCNTs, the current of the electrode modified with Cl-MWCNTs increased by 26 μA (Fig. 2, curves a and b), indicating better electrochemical properties for MWCNTs modified with chloropropyltriethoxysilane than for those modified with hydroxyl groups [26]. The current of the FePP-modified electrode (56 μA) greatly exceeded with that of porphyrin-modified electrode (Fig. 2, curves c and d). Since two pyrrole protons in the porphyrin matrix were replaced by iron to form FePP, the conductivity and electrocatalytic activity of FePP were much greater than those of porphyrin because of the promotion of the electron transfer on the electrode by iron, which accelerates the reaction rate [27]. The highest current (78 μA) was obtained for the electrode modified with Cl/FePP-MWCNTs (Fig. 2, curve e). Furthermore, the Cl/FePP–MWCNTs/GCE is electrochemically stable in a wide potential window and exhibits high conductivity and ion mobility, which is ascribed to the presence of Cl-MWCNTs and FePP [28]. In addition, excellent solubility and adhesion of ionic liquid also increased the sensitivity of Cl/FePP-MWCNTs.[29]

The interfacial characteristics of the charge transfer processes on the electrode surfaces were elucidated by EIS. The impedance spectra, including the high-frequency semicircular portion and low-frequency linear portion, of the bare GCE, Cl-

MWCNTs/GCE, FePP/GCE, Cl/FePP-MWCNTs/GCE, and Cl/FePP-MWCNTs/AChE/GCE are shown in Fig. 3. The semicircular diameter represents the charge transfer resistance (R_{ct}), which dominates the electron transfer kinetics of the redox probe across the electrode interface, while the linear portion is attributed to the diffusion limit [30]. EIS was performed in PBS (pH 7.0) containing $[Fe(CN)_6]^{3-/4-}$ at 5.0 mmol/L and KCl at 0.1 mol/L. The bare GCE exhibited a large semicircle with R_{ct} of 1875 Ω (Fig. 3, curve a), while the R_{ct} values of the FePP/GCE (Fig. 3, curve b), the Cl-MWCNTs/GCE (Fig. 3, curve c), and the Cl/FePP–MWCNTs/GCE (Fig. 3, curve d) were 977, 107, and 70 Ω, respectively. These results indicate that modification with the synthesized Cl/FePP-MWCNTs increased the conductivity of the electrode. The electron transfer at the electrode/solution interface was accelerated by the Cl/FePP-MWCNTs, which enhanced the accessible surface area and increased the electrical conductivity. After immobilization of AChE on the Cl/FePP-MWCNTs/GCE (Fig. 3, curve e), R_{ct} sharply increased because AChE inhibited the electron transfer as a biological macromolecule with low conductivity. Fortunately, R_{ct} of the Cl/FePP-MWCNTs/AChE/GCE was relatively low (583 Ω).

Electrochemical performance of the Cl/FePP-MWCNTs/AChE/GCE biosensor

Figure 4 shows the DPV curves of the AChE/GCE, MWCNTs/AChE/GCE, and Cl/FePP–MWCNTs/AChE/GCE biosensors in 0.1 mol/L PBS (pH 7.0) containing ATCl

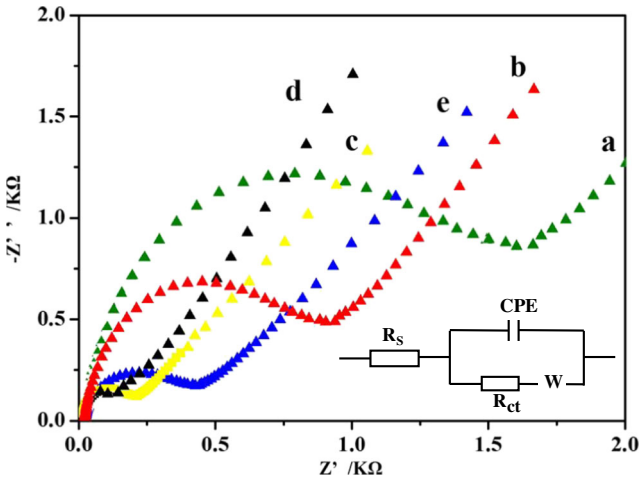

Fig. 3 Electrochemical impedance spectroscopy results for the bare glassy carbon electrode (GCE) (a), Cl-modified multiwalled carbon nanotubes (MWCNTs)/GCE (b), iron porphyrin (FePP)/GCE (c), Cl/FePP-modified MWCNTs/GCE (d), and Cl/FePP-modified MWCNTs/acetylcholinesterase/GCE (e) in 0.1 mol/L phosphate-buffered saline (pH 7.0) containing $[Fe(CN)_6]^{3-/4-}$ at 5.0 mmol/L and KCl at 0.1 mol/L. The inset shows the equivalent circuit. CPE constant phase element, R_{ct} charge transfer resistance R_s, electrolyte resistance, *W* Warburg impedance

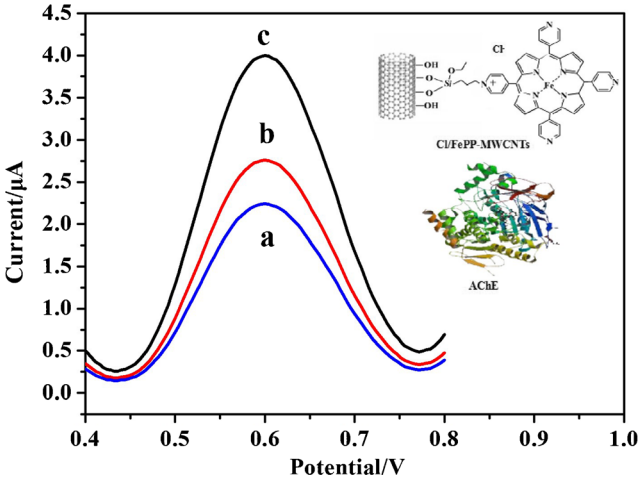

Fig. 4 Differential pulse voltammetry curves of the acetylcholinesterase (AChE)/glassy carbon electrode (GCE) (a), multiwalled carbon nanotubes (MWCNTs)/AChE/GCE (b), Cl/iron porphyrin (FePP)-modified MWCNTs/AChE/GCE (c) biosensors in 0.1 mol/L phosphate-buffered saline (pH 7.0) containing acetylthiocholine chloride at 1.0 mmol/L

at 1.0 mmol. The AChE/GCE successfully catalyzed the hydrolysis of ATCl to generate thiocholine, although the oxidation exhibited a lower peak current on this biosensor than on the bare GCE (Fig. 4, curve a). MWCNTs were used as a "wire" because of their high-speed electron transfer ability. Curve b in Fig. 4 shows that the peak current of the MWCNTs/AChE/GCE was higher than that of the AChE/GCE. FePP has excellent electrochemical properties, which are similar to those of HRP. Curve c in Fig. 4 shows that the peak current of the Cl/FePP-MWCNTs/AChE/GCE was greatly increased compared with that of the MWCNTs/AChE/GCE. This indicates that the Cl/FePP-MWCNTs/AChE/GCE is a novel and efficient biosensor for the sensitive detection of monocrotophos.

The electrochemical properties of the biosensors were further studied by chronoamperometry. ATCl solution was continuously dropped into 0.1 mol/L PBS (pH 7.0) every 40 s to reach a final ATCl concentration in the range from 0 to 20 mmol/L, and the current change was recorded. Figure 5 shows the chronoamperometry curves of the OH-MWCNTs/AChE/GCE, Cl-MWCNTs/AChE/GCE, and Cl/FePP-MWCNTs/AChE/GCE sensors. The response currents of all the biosensors increased stepwise with the gradual addition of ATCl solution, which is correlated with the continuous concentration increase. The sensor responded rapidly to ATCl with a response time of 2 s (time up to 96% of the next steady-state current), which was ascribed to the porous structure of the Cl/FePP-MWCNTs, allowing rapid diffusion of ATCl. The Cl/FePP-MWCNTs/AChE/GCE showed the best response among the three sensors. The inset in Fig. 5 shows the linear calibration curve of the response of the Cl/FePP-MWCNTs/AChE/GCE to ATCl. The current increased linearly in

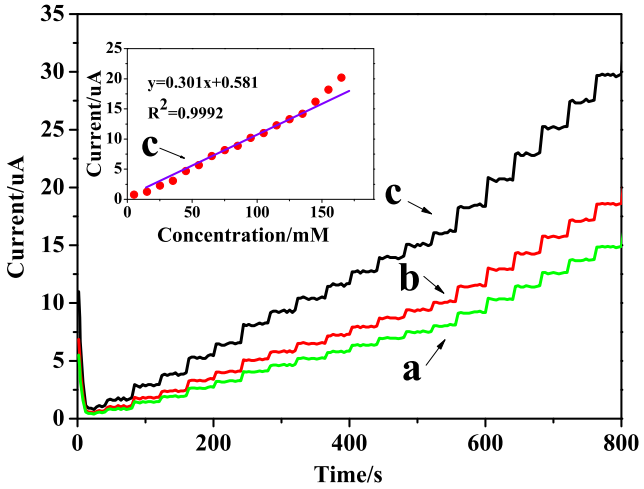

Fig. 5 Typical current–time plots for the acetylcholinesterase (AChE)/glassy carbon electrode (GCE) (a), multiwalled carbon nanotubes (MWCNTs)/AChE/GCE (b), and Cl/iron porphyrin modified MWCNTs/AChE/GCE (c) biosensors on successive additions of acetylthiocholine chloride (ATCl) (0.5, 2.5, 10, and 20 mmol/L) to pH 7.0 phosphate-burred saline under stirring at 0.70 V. The inset shows the calibration plot for the ATCl sensor\

response to increasing ATCl concentration in the range from 0.4 to 1.4 mmol/L. The apparent Michaelis constant (K_M) of the sensor generally reflects the kinetic characteristics of the enzyme and was calculated according to the Lineweaver–Burk equation:

$$\frac{1}{i} = \frac{K_M}{i_m}\left(\frac{1}{C}\right) + \frac{1}{i_m},$$

where i refers to the steady-state current after addition of the substrate, i_m refers to the maximum response current for the saturated substrate, and C refers to the substrate concentration. The calculation reveals an apparent K_M of 1.56 mmol/L, which is lower than the value reported in the literature [31], indicating increased affinity of AChE for the substrate ATCl in the Cl/FePP-MWCNTs/AChE/GCE sensor compared with the previously reported system.

Parameter optimization for the biosensor performance

Enzymatic activity is greatly affected by the pH. To optimize the pH, the pH effect on the sensor response was studied. DPV of the Cl/FePP-MWCNTs/AChE/GCE was performed in PBS of different pH (6.0, 6.5, 7.0, 7.5, 8.0, 8.5, and 9.0; Fig. 6a) containing ATCl at 1.0 mmol/L. The DPV peak current first increased and then decreased with the increase of the pH of PBS and reached its maximum at pH 7.0. This is mainly attributed to the fact that AChE has the highest catalytic activity in a neutral environment [7, 14, 16]. Therefore, pH 7.0 was selected as the optimum pH for PBS in the next experiments.

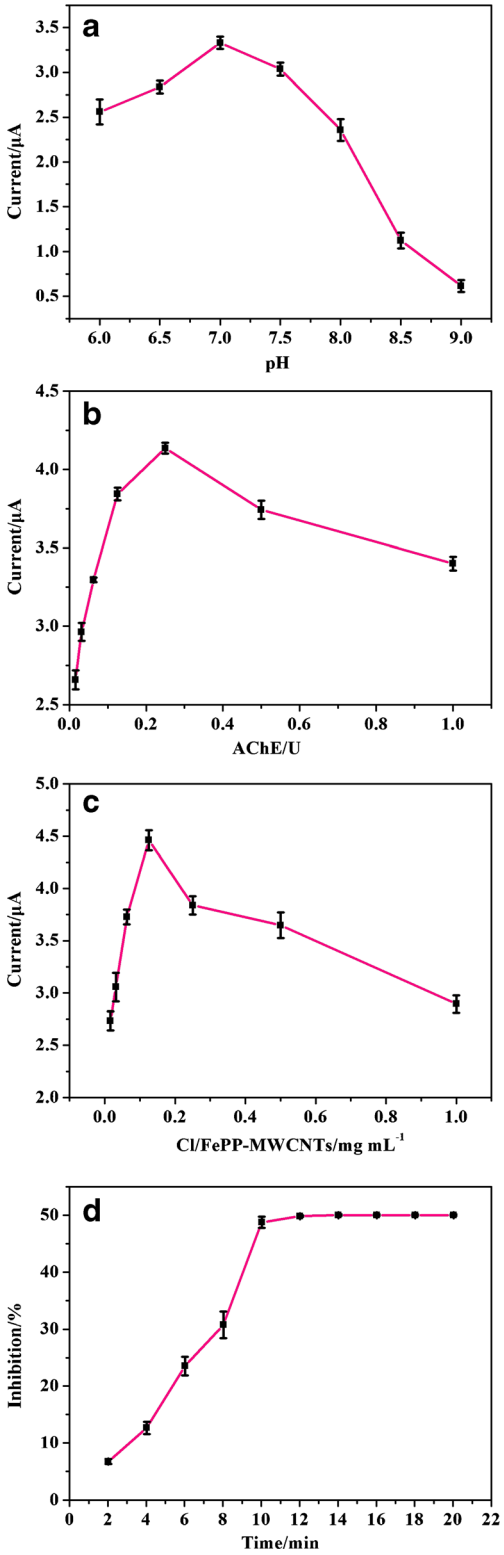

Fig. 6 Effect of **a** pH, **b** acetylcholinesterase (AChE) loading, **c** concentration of the Cl/iron porphyrin (FePP)-modified multiwalled carbon nanotube (MWCNT) nanocomposite, and **d** inhibition time on the current of the biosensor

Furthermore, we studied the effect of AChE loading on the sensor response. DPV curves of the Cl/FePP-MWCNTs/

AChE/GCE containing different amounts of AChE were recorded in PBS (pH 7.0) containing ATCl at 1.0 mmol/L. As shown in Fig. 6b, the peak current achieved its maximum at an AChE amount of 0.25 U. As the enzyme-catalyzed reaction was saturated for small enzyme amounts, the reaction rate increased as the enzyme amount increased. When the enzyme amount was high enough, the substrate amount limited the reaction rate [32]. Moreover, too high enzyme amounts increased the electrode resistance, which impeded the electron transfer.[6] Therefore, 0.25 U was chosen as the optimal amount of AChE in this experiment.

Subsequently, the effect of the amount of Cl/FePP-MWCNT on the sensor performance was studied. DPV of the Cl/FePP–MWCNTs/AChE/GCE was performed with different carrier amounts in PBS (pH 7.0) containing ATCl at 1.0 mmol/L and 0.25 U AChE. As shown in Fig. 6c, the peak current reached its maximum at a carrier concentration of 1 mg/mL, which was attributed to the restricted effective electrode surface area and the growing electron transfer resistance. The carrier coverage of the electrode surface increased as the concentration of the carrier solution increased, but the effective electrode surface area did not increase correspondingly. Hence, the carrier coverage increased resulting in electron transfer resistance worsened. In addition, the AChE adsorption area in the carrier became larger with the increased distribution extent. The greater the extend to which AchE was distributed in the carrier, the more difficult it was to increase the catalytic efficiency for a constant amount of enzyme. Therefore, both the reaction rate and peak current decreased [33].

Monocrotophos inhibited the activity of AChE, and the inhibition was stable after a certain time [34]. Figure 6d presents the results for the experimental optimization of the inhibition time. The Cl/FePP-MWCNTs/AChE/GCE was incubated with 1.0×10^{-9} mol/L monocrotophos standard solution for different times (2–20 min). Within the first 10 min, the inhibition rate increased greatly and reached a stable value of about 50% after 10 min. Therefore, 10 min was chosen as the optimal incubation time for the Cl/FePP-MWCNTs/AChE/GCE.

Detection of monocrotophos with the Cl/FePP-MWCNTs/AChE/GCE biosensor

DPV standard curves of the Cl/FePP-MWCNTs/AChE/GCE were measured in 0.1 mol/L PBS (pH 7.0) containing ATCl at 1.0 mmol/L (Fig. 7), revealing one current peak at 0.6 V. Different DPV peaks were obtained when the sensor was immersed in monocrotophos solutions with different concentrations for 10 min. The inset in Fig. 7 shows the relationship between the monocrotophos concentration and the inhibition rate for the OH-MWCNTs/AChE/GCE, Cl-MWCNTs/AChE/GCE, and Cl/FePP-MWCNTs/AChE/GCE sensors. For all the sensors, the inhibition rate increased with increasing monocrotophos concentration. For the Cl/FePP–MWCNTs/AChE/GCE sensor, curve c exhibits a linear relationship between the inhibition rate and the negative logarithm of the

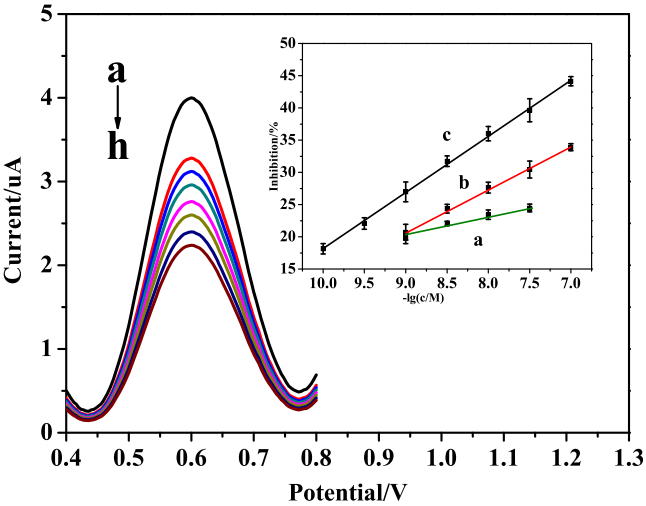

Fig. 7 Differential pulse voltammetry curves of the Cl/iron porphyrin (FePP)-modified multiwalled carbon nanotubes (MWCNTs)/acetylcholinesterase (AChE)/glassy carbon electrode (GCE) biosensor in 0.1 mol/L phosphate-buffered saline (pH 7.0) containing acetylthiocholine chloride at 1.0 mmol/L after incubation with monocrotophos for 10 min. In the inset, curves a, b, and c show the inhibition rates of the OH-modified multiwalled carbon nanotubes (MWCNTs)/acetylcholinesterase (AChE)/glassy carbon electrode (GCE), Cl-modified MWCNTs/AChE/GCE, and Cl/iron porphyrin modified MWCNTs/AChE/GCE biosensors versus the logarithm of monocrotophos concentration, respectively

concentration when the monocrotophos concentration was in the range from 1.0×10^{-10} to 1.0×10^{-7} mol/L, and the corresponding linear equation was y (%) = 1.857–7.7857 log$C$ (R^2 = 0.9987). According to the formula LOD = 3SD/slope (where LOD is the limit of detection and SD is the standard deviation), the detection limit was calculated as 3.2×10^{-11} mol/L. The Cl/FePP-MWCNTs/AChE/GCE biosensor exhibited a wider linear range, lower detection limit, and higher sensitivity relative to the OH-MWCNTs/AChE/GCE and Cl-MWCNTs/AChE/GCE biosensors. The performance of AChE biosensors in the detection of monocrotophos reported in recent years is shown in Table 1 [35–38]. FePP enhanced the electrochemical performance of MWCNTs and promoted the hydrolysis reaction. Moreover, ionic liquids had a wider electrochemical deposition window and enhanced electron transfer efficiency. Together, these factors optimized the detection range and detection limit of the sensor.

Reliability analysis of the biosensor

Cabbage, lettuce, and leek samples were sprayed with monocrotophos insecticide with different concentrations, as described in detail in "Monocrotophos residue detection in real samples." These samples were analyzed with the Cl/FePP-MWCNTs/AChE/GCE biosensor to evaluate its reliability in the detection of monocrotophos in real samples. Table 2 shows high recovery rates in the ranges from 89.0% to 103.0%, from 97.0% to 104.0%, and from 92.0% to 102%,

Table 1 Comparison with other reported biosensors for monocrotophos detection

Electrode material	Linear range (mol L^{-1})	Detection limit (mol L^{-1})	Reference
AChE/Au/graphite	5.0×10^{-5}–4.0×10^{-4}	5.0×10^{-5}	[35]
UCNPs-AuNPs-AChE	1×10^{-13}–5×10^{-8}	1.0×10^{-10}	[36]
AChE/nano-TS-1-Pr-NH_2/GCE	3.6×10^{-10}–3.1×10^{-6}	4.5×10^{-11}	[37]
Pt/ZnO/AChE/chitosan	5×10^{-8}–$4 \times 1\ 0^{-7}$	3.6×10^{-11}	[38]
Cl/FePP-MWCNTs/AChE/GCE	1.0×10^{-10}–1.0×10^{-7}	3.2×10^{-11}	This work

AChE acetylcholinesterase, *AuNPs* gold nanoparticles, *FePP* iron porphyrin, *GCE* glass carbon electrode, *MWCNTs* multiwalled carbon nanotubes, *nano-TS-1-Pr-NH_2* , *UCNPs* upconverting nanoparticles

respectively, for the analyses of cabbage, lettuce, and leek with the Cl/FePP-MWCNTs/AChE/GCE. Especially, relative standard deviation was 4.9% or less, indicating that the Cl/FePP-MWCNTs/AChE/GCE exhibits an anti-interference effect. The biosensor has the advantages of accurate and precise detection, even for the analysis and detection of monocrotophos in environmental samples.

Stability of the Cl/FePP-MWCNTs/AChE/GCE biosensor

The reusability of the Cl/FePP-MWCNTs/AChE/GCE was studied in 1.0 mmol/L ATCl solution after immersion in 1.0 mmol/L monocrotophos solution for 10 min. The biosensor was then dried with an infrared lamp for 20 min and tested again in 1.0 mmol/L ATCl solution. After continuous detection in ATCl solution of the same concentration five times, the relative standard deviation was less than 3.0%, which indicates that the Cl/FePP-MWCNTs/AChE/GCE biosensor has good repeatability. In general, AChE often detached from the electrode surface material because of water tension when the electrode was transferred from one test solution to the other. In this study, adhesive ionic liquid was used to tightly fix the enzyme to the modified electrode, making it difficult for the enzyme to drop off the electrode, thus enhancing the repeatability. In the reproducibility test, six different Cl/FePP-MWCNTs/AChE/GCE biosensors were prepared under the same conditions. The six modified electrodes showed a relative standard deviation of 5.6%, indicating that this sensor has better reproducibility than other reported AChE sensors [39, 40].

Finally, we studied the storage stability of the Cl/FePP-MWCNTs/AChE/GCE after storage at 4 °C. As shown in Fig. 8, the oxidation current decreased slightly after storage for 1 week. After 5 weeks, the oxidation current was 97.8% of its original value. We concluded that the Cl/FePP-MWCNTs/AChE/GCE sensor was stabler than other reported AChE sensors, [41] which was attributed to the presence of FePP. Compared with the inactivation of protease, the FePP sensor was very stable and maintained its high activity even after long-time storage.

Conclusion

Combining the advantages of MWCNTs and ionic liquid, we prepared a novel bienzyme electrode (Cl/FePP-MWCNTs/AChE/GCE) including FePP and AChE for the detection of monocrotophos. CV indicated that the Cl/FePP-MWCNTs/GCE has the highest current value (78 μA), whereas EIS revealed a relatively low R_{ct} of 70 Ω. Furthermore, the Cl/FePP-MWCNTs/GCE was electrochemically stable in a wide potential

Table 2 Determination of monocrotophos in a practical sample

Sample	Number	Added (mol/L)	Found (mol/L)	Mean recovery (%)	RSD (%) (n = 3)
Background control	1	0	0	--	--
Cabbage	1	1.0×10^{-7}	1.02×10^{-7}	102	4.6
	2	1.0×10^{-8}	0.89×10^{-8}	89	3.5
	3	1.0×10^{-9}	1.03×10^{-9}	103	4.0
Lettuce	1	1.0×10^{-7}	1.04×10^{-7}	104	3.3
	2	1.0×10^{-8}	1.01×10^{-8}	101	3.7
	3	1.0×10^{-9}	0.97×10^{-9}	97	3.6
Leek	1	1.0×10^{-7}	1.02×10^{-7}	102	4.9
	2	1.0×10^{-8}	0.92×10^{-8}	92	3.9
	3	1.0×10^{-9}	0.99×10^{-9}	99	4.5

RSD relative standard deviation

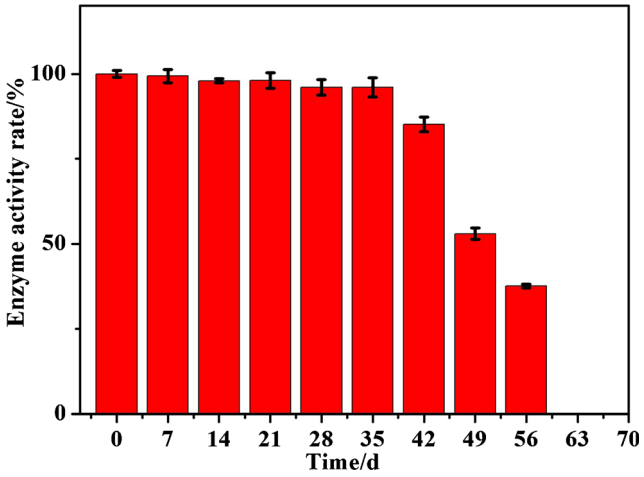

Fig. 8 Enzyme activity rate of the Cl/iron porphyrin modified multiwalled carbon nanotubes/acetylcholinesterase/glassy carbon electrode compared with the initial peak current in 0.1 mol/L phosphate-buffered saline (pH 7.0) containing acetylthiocholine chloride at 1.0 mmol/L at 4 °C

window and had high conductivity. Chronoamperometry of the Cl/FePP-MWCNTs/AChE/GCE revealed K_M of 1.56 mmol/L, indicating good substrate affinity of the Cl/FePP-MWCNTs/AChE/GCE. Under optimal conditions (pH 7.0, AChE loading 0.25 U, carrier amount 1 mg/mL, inhibition time 10 min), the detection limit of the novel biosensor was 3.2×10^{-11} mol/L. Reliability analysis as well as repeatability, reproducibility, and storability tests showed that the biosensor has excellent stability and exhibits anti-interference. Together, the experimental results demonstrate that the novel sensor is very stable and highly active for the detection of monocrotophos.

Acknowledgements The work was funded by the National Natural Science Foundation of China (no. 21406093), the Natural Science Foundation of Jiangsu Province (no. BK20140529), the Key University Science Research Project of Jiangsu Province (no. 14KJB530001), the China Postdoctoral Science Foundation (no. 2014M550271), and the Priority Academic Program Development of Jiangsu Higher Education Institutions.

Compliance with ethical standards

Conflict of interest The authors declare no that they have no competing interests.

References

1. Tan MJ, Hong ZY, Chang MH, Liu CC, Cheng HF, Loh XJ. Metal carbonyl-gold nanoparticle conjugates for highly sensitive SERS detection of organophosphorus pesticides. Biosens Bioelectron. 2017;96:167–72.
2. Mendieta-Reyes NE, Díaz-García AK, Gómez R. Simultaneous electrocatalytic CO_2 reduction and enhanced electrochromic effect at WO3 nanostructured electrodes in acetonitrile. ACS Catal. 2018;8:1903–12.
3. Ragno D, Carmine GD, Brandolese A, Bortolini O, Giovannini PP, Massi A. Immobilization of privileged triazolium carbene catalyst for batch and flow stereoselective umpolung processes. ACS Catal. 2017;7:6365–75.
4. Gong J, Wang X, Li X, Wang K. Highly sensitive visible light activated photoelectrochemical biosensing of organophosphate pesticide using biofunctional crossed bismuth oxyiodide flake arrays. Biosens Bioelectron. 2012;38:43–9.
5. Cui HF, Wu WW, Li MM, Song X, Lv Y, Zhang TT. A highly stable acetylcholinesterase biosensor based on chitosan-TiO_2-graphene nanocomposites for detection of organophosphate pesticides. Biosens Bioelectron. 2018;99:223–9.
6. Sgobbi LF, Sas M. Functionalized polyacrylamide as an acetylcholinesterase-inspired biomimetic device for electrochemical sensing of organophosphorus pesticides. Biosens Bioelectron. 2017;100:290–7.
7. Zheng Q, Yu Y, Fan K, Ji F, Wu J, Ying Y. A nano-silver enzyme electrode for organophosphorus pesticide detection. Anal Bioanal Chem. 2016;408:1–9.
8. Tran T, Mulchandani A. Carbon nanotubes and graphene nano field-effect transistor-based biosensors. Trends Anal Chem. 2016;79:222–32.
9. Ahmad R, Khare SK. Immobilization of aspergillus niger cellulase on multiwall carbon nanotubes for cellulose hydrolysis. Bioresour Technol. 2017;252:72–5.
10. Neto SA, Silva RGD, Milton RD, Minteer SD, Andrade ARD. Hybrid bioelectrocatalytic reduction of oxygen at anthracene-modified multi-walled carbon nanotubes decorated with $Ni_{90}Pd_{10}$ nanoparticles. Electrochim Acta. 2017;251:195–202.
11. Giroud F, Sawada K, Taya M, Cosnier S. 5,5-Dithiobis(2-nitrobenzoic acid) pyrene derivative-carbon nanotube electrodes for NADH electrooxidation and oriented immobilization of multicopper oxidases for the development of glucose/O_2 biofuel cells. Biosens Bioelectron. 2017;87:957–63.
12. Chen B, Wang Y, Li C, Fu L, Liu X, Zhu Y. A Cr_2O_3/MWCNTs composite as a superior electrode material for supercapacitor. RSC Adv. 2017;7:25019–24.
13. Kaur N, Thakur H, Prabhakar N. Conducting polymer and multi-walled carbon nanotubes nanocomposites based amperometric biosensor for detection of organophosphate. J Electroanal Chem. 2016;775:121–8.
14. Yu G, Wu W, Zhao Q, Wei X, Lu Q. Efficient immobilization of acetylcholinesterase onto amino functionalized carbon nanotubes for the fabrication of high sensitive organophosphorus pesticides biosensors. Biosens Bioelectron. 2015;68:288–94.
15. Manoj D, Theyagarajan K, Saravanakumar D, Senthilkumar S, Thenmozhi K. Aldehyde functionalized ionic liquid on electrochemically reduced graphene oxide as a versatile platform for covalent immobilization of biomolecules and biosensing. Biosens Bioelectron. 2018;103:104–12.
16. Gholivand MB, Karimian N, Torkashvand M. A highly sensitive electrochemical OPs biosensor based on electrodeposition of Au–Pd bimetallic nanoparticle onto functionalized graphene modified glassy carbon electrode. Anal Methods. 2015;7:3903–11.
17. Horiuchi T, Torimitsu K, Yamamoto K, Niwa O. On-line flow sensor for measuring acetylcholine combined with microdialysis sampling probe. Electroanalysis. 2010;9:912–6.
18. Zhou Y, Huang X, Zhang W, Ji Y, Chen R, Xiong Y. Multi-branched gold nanoflower-embedded iron porphyrin for colorimetric immunosensor. Biosens Bioelectron. 2017;102:9–16.
19. Ji HB, Yuan QL, Zhou XT, Pei LX, Wang LF. Highly efficient selective oxidation of alcohols to carbonyl compounds catalyzed by ruthenium (III) meso-tetraphenylporphyrin chloride in the presence of molecular oxygen. Bioorg Med Chem Lett. 2007;17:6364–8.

20. Ren TZ, Yuan ZY, Su BL. Encapsulation of direct blue dye into mesoporous silica-based materials. Colloids Surf A Physicochem Eng Asp. 2007;300:79–87.
21. Carrasco PM, Montes S, García I, Borghei M, Jiang H, Odriozola I. High-concentration aqueous dispersions of graphene produced by exfoliation of graphite using cellulose nanocrystals. Carbon. 2014;70:157–63.
22. Gao L, Deng K, Zheng J, Liu B, Zhang Z. Efficient oxidation of biomass derived 5-hydroxymethylfurfural into 2,5-furandicarboxylic acid catalyzed by Merrifield resin supported cobalt porphyrin. Chem Eng J. 2015;270:444–9.
23. Cui HF, Wu WW, Li MM, Song X, Lv Y, Zhang TT. A highly stable acetylcholinesterase biosensor based on chitosan-TiO_2-graphene nanocomposites for detection of organophosphate pesticides. Biosens Bioelectron. 2017;99:223–9.
24. Bidari A, Ganjali MR, Norouzi P. Sample preparation method for the analysis of some organophosphorus pesticides residues in tomato by ultrasound-assisted solvent extraction followed by dispersive liquid-liquid microextraction. Food Chem. 2011;126:1840–4.
25. Wang F, Ma S, Si Y, Dong L, Wang X. Interaction mechanisms of antibiotic sulfamethoxazole with various graphene-based materials and multiwall carbon nanotubes and the effect of humic acid in water. Carbon. 2017;114:671–8.
26. Uwimbabazi E, Mukasekuru MR, Sun X. Glucose biosensor based on a glassy carbon electrode modified with multi-walled carbon nanotubes-chitosan for the determination of beef freshness. Food Anal Methods. 2017;10:1–10.
27. Rahmanian R, Mozaffari SA, Amoli HS, Abedi M. Development of sensitive impedimetric urea biosensor using DC sputtered nano-ZnO on TiO_2 thin film as a novel hierarchical nanostructure transducer. Sensors Actuators B Chem. 2017;256:760–74.
28. Lu L, Huang X, Qu Y. Improvement of carbon paste-based enzyme electrode using a new ionic liquid [Pmim][PF_6] as the binder. J Solid State Electrochem. 2012;16:3299–305.
29. Fan Y, Hu G, Zhang T, Dong X, Zhong Y, Li X. Determination of glucose in food by the ionic liquid and carbon nanotubes modified dual-enzymatic sensors. Food Anal Methods. 2016;9:2491–500.
30. Zhou L, Zhang X, Ma L. Acetylcholinesterase/chitosan-transition metal carbides nanocomposites-based biosensor for the organophosphate pesticides detection. Biochem Eng J. 2017;128:243–249.
31. Santos CS, Pawlak V, Fujiwara ST. Acetylcholinesterase biosensor based on Paman self-assembled monolayer-modified gold electrode, ECS Meeting. (2014);433. http://ma.ecsdl.org/content/MA2014-01/5/433.abstract. Accessed 1 May 2014
32. Dong J, Wang X, Qiao F, Liu P, Ai S. Highly sensitive electrochemical stripping analysis of methyl parathion at MWCNTs–CeO_2–Au nanocomposite modified electrode. Sensors Actuators B Chem. 2013;186:774–80.
33. Wei M, Feng S. Amperometric determination of organophosphate pesticides using a acetylcholinesterase based biosensor made from nitrogen-doped porous carbon deposited on a boron-doped diamond electrode. Microchim Acta. 2017;184:3461–8.
34. Zheng Y, Liu Z, Jing Y, Li J, Zhan H. An acetylcholinesterase biosensor based on ionic liquid functionalized graphene–gelatin-modified electrode for sensitive detection of pesticides. Sensors Actuators B Chem. 2015;210:389–97.
35. Dimcheva N, Horozova E, Ivanov Y. Self-assembly of acetylcholinesterase on gold nanoparticles electrodeposited on graphite. Cent Eur J Chem. 2013;11:1740–8.
36. Long Q, Li H, Zhang Y, Yao S. Upconversion nanoparticle-based fluorescence resonance energy transfer assay for organophosphorus pesticides. Biosens Bioelectron. 2015;68:168–74.
37. Kaur B, Srivastava R, Satpati B. Nanocrystalline titanosilicate–acetylcholinesterase electrochemical biosensor for the ultra-trace detection of toxic organophosphate pesticides. Chemelectrochem. 2015;2:1164–73.
38. Sundarmurugasan R, Gumpu MB, Ramachandra B. Simultaneous detection of monocrotophos and dichlorvos in orange samples using acetylcholinesterase–zinc oxide modified platinum electrode with linear regression calibration. Sensors Actuators B Chem. 2016;230:306–13.
39. Zhao H, Ji X, Wang B. An ultra-sensitive acetylcholinesterase biosensor based on reduced graphene oxide-Au nanoparticles-β-cyclodextrin/Prussian blue-chitosan nanocomposites for organophosphorus pesticides detection. Biosens Bioelectron. 2015;65:23–30.
40. Ma L, Zhou L, He Y. Hierarchical nanocomposites with an N-doped carbon shell and bimetal core: novel enzyme nanocarriers for electrochemical pesticide detection. Biosens Bioelectron. 2018;121:166–73.
41. Zhang Q, Xu Q, Guo Y, Sun X, Wang X. Acetylcholinesterase biosensor based on the mesoporous carbon/ferroferric oxide modified electrode for detecting organophosphorus pesticides. RSC Adv. 2016;6:24698–703.